Investigation of the Influence of Temperature and Annealing on the Radiation Hardness of Silicon Mach–Zehnder Modulators

Andrea Kraxner, Stephane Detraz, Lauri Olantera, Carmelo Scarcella, Christophe Sigaud, Csaba Soos, Jan Troska, and Francois Vasey

***Abstract*— Optical links are vital components in the data transmission systems of high energy physics (HEP) experiments at CERN. With the ever higher beam fluxes achieved by the Large Hadron Collider, the optical components have to withstand higher radiation levels and handle ever-increasing data volumes. To face these challenges, the use of silicon photonics (SiPh) Mach–Zehnder modulators (MZMs) in the next generation of optical transceivers for HEP experiments is currently being investigated. In this paper, the dependence of the radiation hardness of custom-designed SiPh MZMs on temperature is reported, including the observed improvement in radiation tolerance at low operating temperatures that are closer to the typical temperatures found in HEP experiments. Furthermore, postirradiation annealing measurements of the devices were performed. An effective annealing method has been found by applying a forward current to the MZMs, leading to an almost immediate and full recovery of the device after irradiation up to 3 MGy. This enhanced device recovery method could effectively increase the radiation hardness tremendously in applications with low dose rates and periodic shutdown times.**

***Index Terms*— Annealing, CERN, high energy physics (HEP), ionizing radiation, Large Hadron Collider (LHC), Mach–Zehnder modulator (MZM), radiation damage, silicon photonics (SiPh), X-ray.**

I. Introduction

AT THE Large Hadron Collider (LHC) at CERN, beams of high energy (14 TeV) protons are brought into collision to achieve conditions similar to those immediately after the Big Bang. These conditions are used to study the fundamental properties of matter in high energy physics (HEP) experiments. The desire of the high energy physicists to study ever rarer processes requires the particle collision rate to be increased with every generation of experiment, generating ever larger quantities of data that need to be transmitted from the experiment to their associated processing electronics. Optical links have become ubiquitous in this data transmission path due to their many advantages over copper (low mass, high capacity, immunity to electromagnetic interference, and so on). The high collision rate also produces ever higher radiation levels, both ionizing and nonionizing, that must be tolerated by all components placed within the experiments. As an example, with the upgrade of the LHC to high luminosity (HL-) LHC [1], components to be installed in the upgrading experiments will have to withstand a 1-MeV equivalent neutron fluence of at least 2×10^{15} n/cm^2 and a total ionizing dose (TID) level of 1 MGy over the operational lifetime of ten years.So far, links based on both single-mode edge-emitting lasers [2] and multimode vertical-cavity surface-emitting lasers [3] are in use in the experiments at CERN. The drawback of laser diode-based technologies is their degradation due to displacement damage from particle fluence [4]. Because of this, alternatives for the most exposed areas in the HL-LHC experiments are being investigated for data transmission systems operating up to 10 Gb/s. Silicon photonics (SiPh) Mach–Zehnder modulators (MZMs) are a possible option. In SiPh-based optical links, the possibility to use remotely located single-mode laser sources reduces the requirement on the radiation hardness of the light source. Furthermore, the possibility to cointegrate SiPh devices with electronic drivers [5]–[7] and silicon particle sensors could lead to a highly integrated detector system in HEP experiments. This would bring additional benefits by decreasing the power consumption, size, and costs while increasing the functionality. As the active material would be the same as used in the silicon particle sensor [8], [9], a similar level of radiation hardness could be expected. The previous work has shown that SiPh MZMs are relatively insensitive to neutron radiation [10], [11], but they show strong degradation with the ionizing X-ray radiation [12]. Understanding of the radiation damage mechanisms in SiPh MZMs led to the design of custom MZMs [13] that have been shown to be significantly more radiation tolerant [14]. Fully optimized devices have been shown to be able to withstand a TID of up to 3.2 MGy (unbiased measurement), albeit with a larger initial device insertion loss. In this paper, we show that even higher TID levels can be reached when decreasing the operating temperature and by including specific annealing procedures between the irradiation steps. *In situ* measurement results are presented, comparing the influence of different temperatures during the irradiation on the radiation resistance. We also show the effect of room temperature beneficial annealing as well as indications of reverse (anti)annealing. Finally, the effect of

Manuscript received February 8, 2018; revised March 26, 2018; accepted April 3, 2018. Date of publication April 6, 2018; date of current version August 15, 2018.

The authors are with the Experimental Physics Department, CERN, CH-1211 Geneva, Switzerland (e-mail: andrea.kraxner@cern.ch).

Color versions of one or more of the figures in this paper are available online at http://ieeexplore.ieee.org.

Digital Object Identifier 10.1109/TNS.2018.2823863

This work is licensed under a Creative Commons Attribution 3.0 License. For more information, see http://creativecommons.org/licenses/by/3.0/

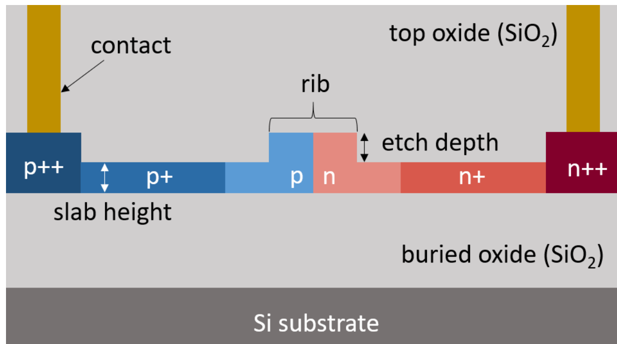

Fig. 1. Cross section through the depletion-type SiPh phase shifter with the lateral p-n junction used for this paper.

applying a forward bias to the modulator structure is shown to provide beneficial annealing.

II. Test Samples and Measurement Procedures

With the knowledge gained in [14], further experiments were performed using the same customized silicon MZMs described there and in greater detail in [13]. The cross section of the modulator used is shown in Fig. 1, highlighting the different doping regions and design parameters. The design parameters varied to investigate their effect on the overall device radiation tolerance are the etch depth (silicon slab height) and the p- and n-doping concentrations in the rib region (nominal doping and twice the nominal doping). Two etch depths were investigated: 160 nm (deep etch) and 70 nm (shallow etch). The nominal doping concentration in the rib region is not known precisely, but it is expected to be in the region of 10^{18} cm^{-3}. The higher doping concentration in the rib region was shown to make the modulator more radiation resistant at the expense of higher optical losses in the waveguides [14]. The contact (n++/p++) and the intermediate (n+/p+) doping concentrations were kept constant. The waveguide rib width was 450 nm and the height was 220 nm in all customized designs. The phase-shifter length was 1.9 mm and the path length difference was chosen to be 30 μm. The test chips were produced on 200-mm silicon-on-insulator wafers in the IMEC ISIPP25G technology as part of a Multi Project Wafer run offered by ePIXfab [15]. The thickness of the top oxide was 1 μm.

In order to investigate the response of the various structures to ionizing radiation, assembled chips were placed in a Seifert RP149 X-ray irradiator and the phase shift and the current–voltage characteristics (I–V) of the MZMs were measured *in situ* during irradiation. The irradiation was not interrupted to perform measurements that were carried out and recorded periodically at the fixed time intervals during the entire length of a given irradiation period. To measure the phase shift generated by an individual MZM arm, light from a superluminescent diode (SLED) was coupled into and out of the chip via optical fibers that were pigtailed to the chip and aligned to grating couplers. The transmission spectra were recorded periodically with a *Yokogawa AQ6370B* Optical Spectrum Analyser as a function of reverse bias voltage. Fig. 2 shows a block diagram of the measurement setup, and Fig. 3 shows the example transmission spectra with 0- and −3-V reverse bias as well as the spectrum of the SLED without device under test (DUT). The low optical power in Fig. 3 can be explained by losses due to coupling (around 3 dB for each grating coupler) and losses through the phase shifter which are about 3.8 (7.6) dB mm^{-1} for nominally (twice-nominally) doped devices [16]. In addition to the on-chip losses, loss is introduced by the measurement setup that includes two optical switches. Due to the polarization sensitivity of the grating couplers, a manual three-paddle polarization controller was used to optimize the coupling efficiency. However, as only one polarization controller was used for five different devices, it was not possible to achieve optimal polarization for all five DUTs simultaneously and resulting the tradeoff in coupling efficiency among the devices lead to further losses in the system.

The following fitting function was used to extract the phase shift from the measured spectra:

$$P_{\text{out}} = y_0 + A \exp\left(-\left(\frac{\lambda - \lambda_{\text{env}}}{\sigma_{\text{env}}}\right)^2\right) \text{Sin}\left(\frac{(\lambda - \lambda_0)\pi}{\text{FSR}}\right)^2 \quad (1)$$

where A, λ_{env}, and σ_{env} are the amplitude, center wavelength, and width, respectively, of a Gaussian-like convolution of the SLED spectrum including the grating coupler transfer function. y_0 is an offset parameter and λ_0 is the position of a transmission minima. Using the values obtained from this fit of a spectrum measured at voltage V_1, the wavelength shift $\Delta\lambda$ at this voltage with respect to 0 V can be calculated as

$$\Delta\lambda = \lambda_0\Big|_{V_1} - \lambda_0\Big|_{0V}. \quad (2)$$

Using the wavelength shift $\Delta\lambda$ and the free spectral range of the transmission spectra at different bias voltages, the phase shift $\Delta\Phi$ in π/mm was calculated taking the device length L into account

$$\Delta\Phi = \frac{2\Delta\lambda}{\text{FSR} \cdot L}. \quad (3)$$

For the following results, three different measurement procedures were used in order to investigate the influence of device biasing during and after irradiation. The bias conditions for one measurement cycle for one arm of an example device for the three measurement procedures are shown in Fig. 4, where the applied voltage is plotted versus measurement time. The measurement procedure used in all our previous works (procedure 1) includes the measurement of the I–V of the phase shifter of each modulator arm. Voltages from 1 V forward to −6 V reverse were applied in 0.2-V steps. After the I–V, the transmission spectra at 0, −1, −2, and −3 V were recorded. During the idle period between the measurements, a given MZM arm was biased at a constant reverse voltage of −3 V with the aim of reproducing a typical operating condition of an MZM in an optical link. However, for practical reasons, it was necessary to leave the connections of the idle device arms floating, while I–V was measured for another arm. These floating periods are indicated by the gap in Fig. 4 for measurement procedure 1. In the second procedure (Fig. 4, procedure 2), no I–V was taken and it was not necessary to keep the device floating at any time during the measurement.

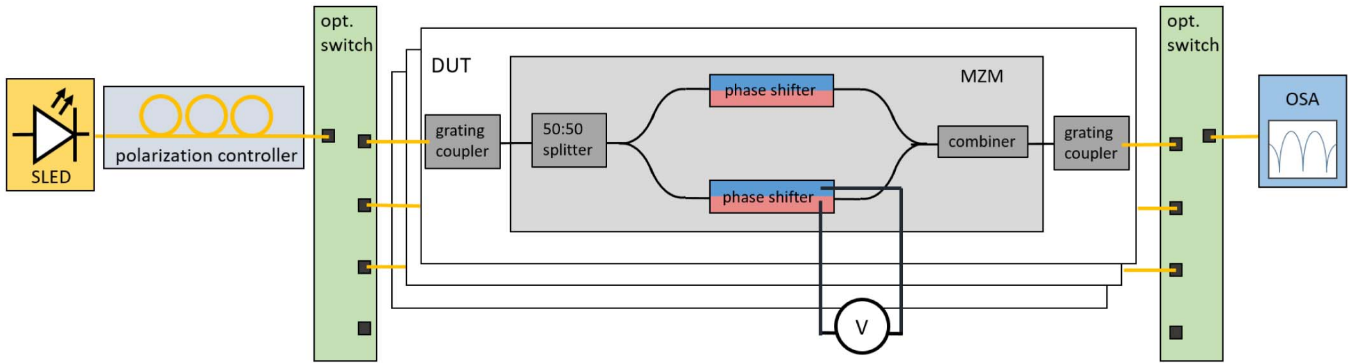

Fig. 2. Schematic of the measurement setup.

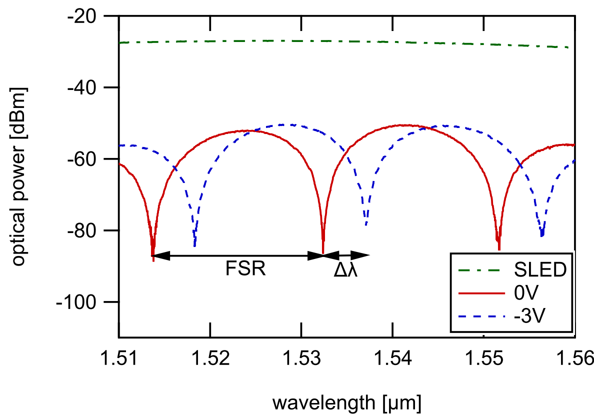

Fig. 3. SLED output spectrum without DUT compared with MZM transmission spectra at 0 and −3 V. Deep-etch MZM with nominal doping.

In addition, this leads to an absence of a forward bias throughout the whole measurement, making this procedure the one closest to application operation. In the third procedure (procedure 3), again no I–V was taken, but a forward bias step was included. A forward current of 2 mA (corresponding to a voltage of 0.9 V) was applied to each modulator arm for 1 min in each measurement cycle. The time between two measurement cycles is shown in Fig. 4.

The chips were irradiated at a constant dose rate of 13.13 Gy s^{-1} with a peak X-ray energy of 10 KeV. The setup of the irradiator was produced a roughly circular beam spot at the DUT, approximately 4 mm in diameter, within which the variation of the beam intensity was within 20% of the peak value. A p-i-n diode was used to calibrate the dose rate at the DUT position for several I–V settings of the X-ray tube with a cross calibration being done using dosimetry films. The arrangement of the various device types on the test chip made it possible to irradiate all tested device types at the same time. A thermal chuck was used to stabilize and control the temperature during irradiation. The chip temperature was recorded in every measurement cycle. Irradiation experiments were performed at room temperature (25 °C), 0 °C and −10 °C for devices with nominal doping and with twice the nominal doping. The annealing behavior was first measured immediately after turning OFF the irradiation source and again after some storage time which varied from sample to sample.

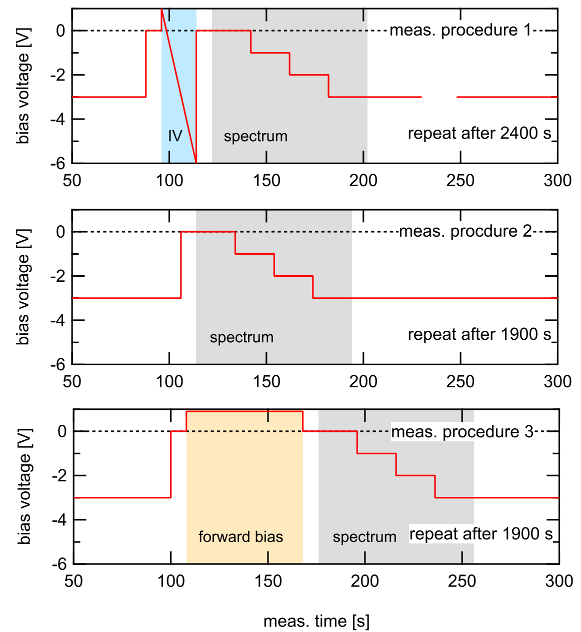

Fig. 4. Bias level as a function of measurement time showing one cycle for one arm of one MZM for the three different measurement procedures compared in this paper.

III. Experimental Results and Discussion

As a first comparison, the radiation hardness of a shallow-etch and a deep-etch device at room temperature is shown in Fig. 5 for a reverse bias of −1, −2, and −3 V. The phase shift is plotted as the relative change to the preirradiation value measured at the same temperature. The first value plotted corresponds to the first measurement performed during irradiation, which is done at some kilograys depending on the device. Because of an increase in phase shift at low TID levels, before the phase shift starts to decrease, the values do not start from unity but are higher than the preirradiation values. As previously reported [14], shallow-etch devices can withstand a higher radiation dose before the phase shift starts to decrease compared with deep-etch devices, compatible with the hypothesis for radiation-induced interface charge build up being responsible for the observed changes in phase shift. The phase shift at −1 V of the deep-etch device is decreased to 50% of its preirradiation value at a TID of approximately

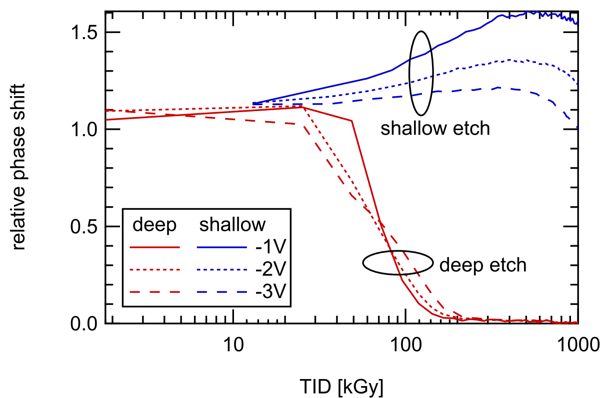

Fig. 5. Relative phase shift for −1, −2, and −3 V of custom-design deep- and shallow-etch MZMs with twice the nominal doping. Measurement performed at room temperature using measurement procedure 1.

70 kGy, while the phase shift of the shallow-etch device begins to degrade above 500 kGy. Furthermore, the −3-V phase shift reaches its preirradiation value for the shallow-etch device following the initial increase only at the end of the irradiation at 1 MGy. The initial increase of the phase shift before the onset of degradation can be explained by the lowering of the doping concentration on the p-side of the device due to trapped holes at the Si–SiO_2 interface, resulting in higher phase shift until the point of pinchoff [14], [17]. After pinchoff occurs, it becomes impossible to change the carrier concentrations in the waveguide region by applying a voltage across the diode and there is no longer any visible phase shift.

A. Temperature Dependence

The change in phase shift with TID at −1 V is shown for room temperature, 0 °C and −10 °C in Fig. 6(a) for a deep-etch device and in Fig. 6(b) for a shallow-etch device. Fig. 6(a) and (b) clearly shows that the lower the temperature, the higher the tolerance to TID is. The radiation resistance of deep-etch devices increases by a factor of 3.6 at 0 °C and 7 at −10 °C with respect to the room temperature measurement. In the case of the shallow-etch devices, the improvement is hard to quantify as no decrease in the phase shift was measured for 0 °C and −10 °C within the irradiation period. The improvement of the radiation tolerance at lower temperature can be explained by the reduction in hole mobility with decreasing temperature. Reduced hole mobility implies that the rate at which deep traps are filled and interface traps build up is lower at lower temperatures, leading to the observed higher resistance to TID. Inside the innermost regions of an HEP experiment, temperatures down to −30 °C are found, indicating that in the final application, even higher radiation resistance than measured here can be expected.

B. Room Temperature Annealing

To examine the postirradiation behavior, annealing measurements were performed for samples with nominal and twice the nominal doping. Measurements were performed using procedure 1 right after irradiation at the irradiation temperature and after raising the device temperature back to room temperature. Further measurements were done at room temperature after multiple months of unbiased storage at room temperature, again using procedure 1. For a sample with nominal doping that was irradiated up to 3.1 MGy at −10 °C, postirradiation measurements were first performed right after irradiation, starting at the irradiation temperature of −10 °C. After 24 h, the temperature was changed to room temperature without stopping the measurement. The temperature change was performed in the waiting period between two measurement points and was settled when the next measurement point was taken. After 4 1/2 months of unbiased storage at room temperature with all connectors shorted, another 45 h of measurement were performed at room temperature. The irradiation and postirradiation changes in phase shift relative to the preirradiation value are shown in Fig. 7 for a shallow-etch and a deep-etch device. In the first part of the plot, the irradiation up to a dose of 3.1 MGy is shown. In the second part, a first measurement period without irradiation at −10 °C and room temperature is shown, followed by the second measurement period without irradiation after 4 1/2 months. In the first measurement period, it can be seen that immediately after the irradiation, the phase shift starts to decrease for the shallow-etch device, which represents a reverse annealing effect. A jump to higher values when the temperature was increased was observed, followed by a faster decrease (reverse annealing) compared with the measurement at −10 °C. The mechanism for a phase-shift increase when increasing the temperature remains elusive, whereas the faster decrease at higher temperature can be explained through an increase in carrier mobility with increasing temperature. The second measurement period after several months shows a significant jump to lower phase-shift values and saturates around 80% of the preirradiation value. These results indicate a reverse annealing effect after the initial increase in phase shift due to irradiation. The reverse annealing effect also seems to be active when the sample is not biased. In the case of the deep-etch device, no change or recovery of the phase shift can be seen during the first measurement period. In the second measurement period, the phase shift starts to reappear already after 5 h of measurement, and after 20 h, the phase shift at −1 V starts to saturate at 80% of the preirradiation value. The phase shift at −2 and −3 V settles between 60% and 75% within the measurement time. The large difference in the final value between the different bias voltages suggests that the value may still increase with a longer annealing time. A similar measurement was performed at a sample with twice the nominal doping irradiated up to 3 MGy at 0 °C. In this case, 80 h of measurement were performed shortly after irradiation without any recovery of the deep-etch devices. Further annealing measurements were performed after three months of storage and the phase shift started to recover after 35 h. Also, in this case, the phase-shift values of deep- and shallow-etch devices settled to 80% of the preirradiation value. The jumps in between measurements and the fast recovery after several months of storage indicate that there is an annealing effect after irradiation which does not depend on the biasing of the sample but on time. However, the fact that the actual recovery appears, while the device that is being measured leads to the

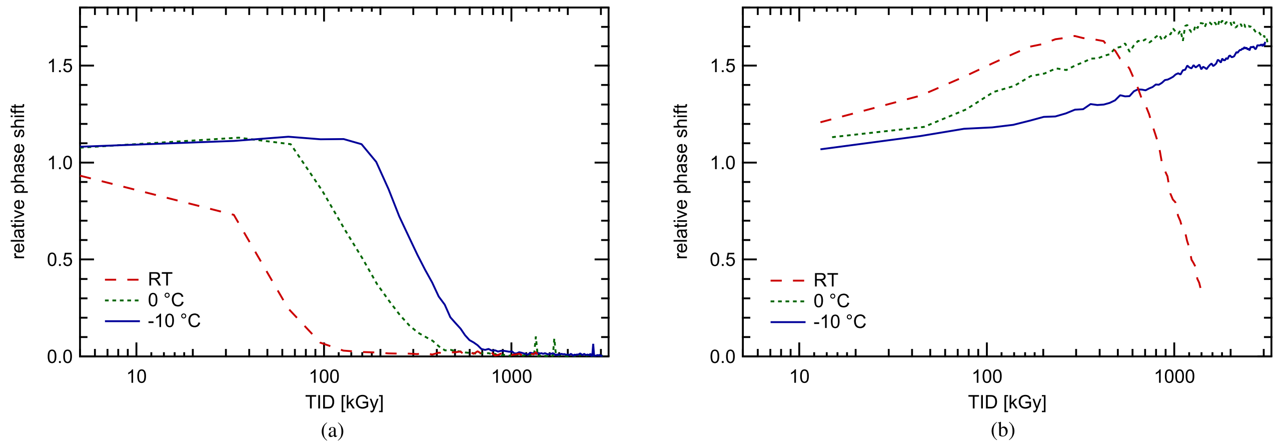

Fig. 6. Temperature dependence of phase-shift change with TID at −1 V for (a) deep- and (b) shallow-etch devices with nominal doping concentration. Measurement procedure 1 was used.

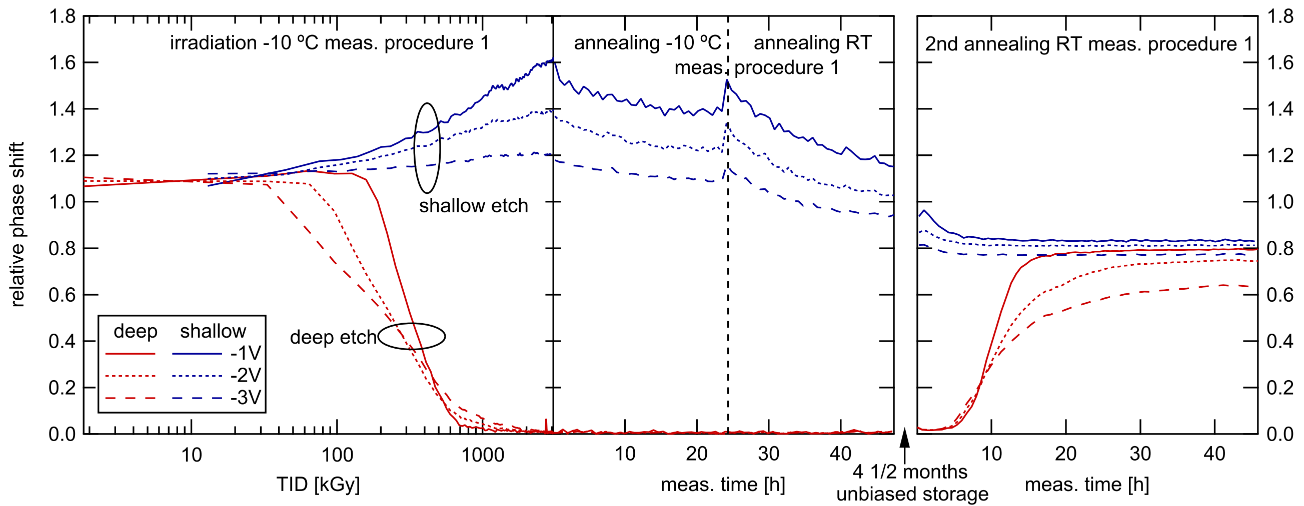

Fig. 7. Relative phase shift for −1, −2, and −3 V of custom shallow- and deep-etch MZMs with nominal doping. First part: irradiation at −10 °C. Second part: annealing measurement at −10 °C and room temperature right after irradiation. Last part: room temperature annealing after 4 1/2 months. All measurements were performed using measurement procedure 1.

conclusion that the annealing effect observed in this test cannot be solely due to temperature but also strongly depends on the biasing conditions. Comparing the two cases, the speed of recovery seems to be dependent on the time that passed since the irradiation and also on the TID that the sample was exposed to.

C. Forward Bias Annealing

In Section III-B, the annealing effect during measurements at room temperature was discussed. The observation that measuring I–V increases the radiation tolerance during the irradiation led to further experiments during which a significantly more effective annealing method was found. A full recovery of the phase shift of an irradiated sample was obtained by applying a forward bias to the modulator. For a better control of the current flowing through the junction, a fixed forward current was applied instead of a forward voltage. The speed of the annealing depends on the magnitude of the current applied to the junction. While a current of 30 mA leads to a recovery of the phase shift immediately after turning on the power supply, approximately 1 min is required to achieve the same effect using a current of 2 mA. With this knowledge, it can be assumed that the effect responsible for the recovery observed in the room temperature measurements presented in Fig. 7 could be the short period of forward bias applied when periodically measuring I–V. This effect was first observed in the devices that were already annealed and stored for three months, similar to the devices shown in Section III-B. In a next step, the influence of forward bias annealing on the phase-shift change during irradiation and annealing right after irradiation was investigated. In Fig. 8, the phase-shift change for a deep- and a shallow-etch device is shown. In these measurements, procedure 2 was used and no forward bias at all (no I–V) was applied during irradiation and annealing. Comparing the phase-shift change during irradiation to measurement results under the same condition but including I–V measurement (Fig. 5, measurement procedure 1), a slightly lower radia-

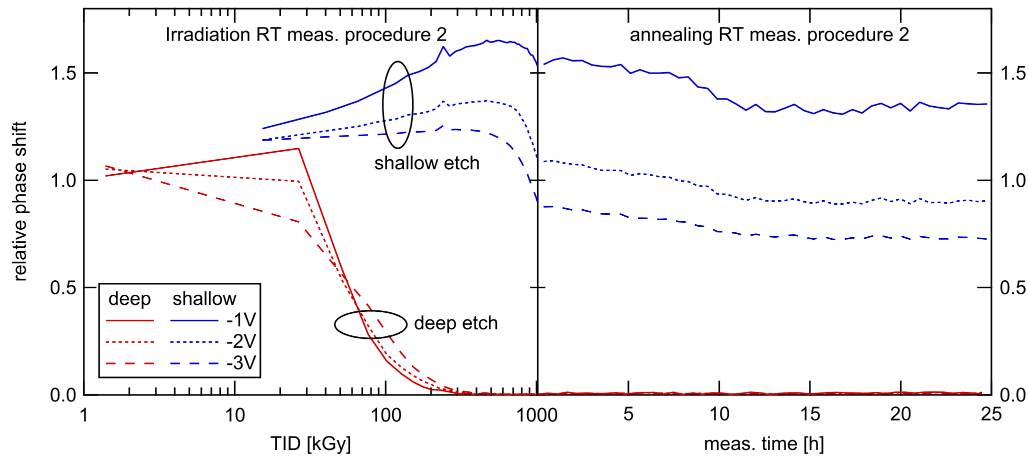

Fig. 8. Relative phase shift for −1, −2, and −3 V of custom-design deep- and shallow-etch MZMs with twice the nominal doping. Measurements performed at room temperature. First part: irradiation. Second part: annealing at room temperature without forward current. Measurement procedure 2 was used for these measurements.

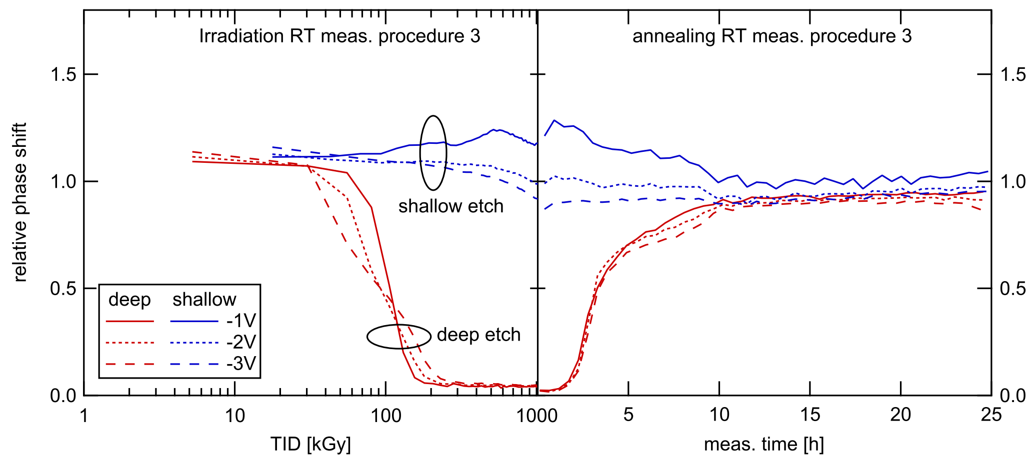

Fig. 9. Phase shift for −1, −2, and −3 V of custom-design deep- and shallow-etch MZMs with twice the nominal doping. Measurements performed at room temperature. First part: irradiation. Second part: annealing at room temperature with 1 min of 2-mA forward current in every measurement. Measurement procedure 3 was used for these measurements.

tion hardness was observed. This is in accordance with the assumption of a small annealing effect due to the forward bias applied during the I–V measurement. The annealing behavior is shown in the second part of Fig. 8. Depending on the applied reverse voltage when modulating, the phase shift of the shallow-etch devices settles between 70% and 140% within the measured annealing time, while there is no phase-shift recovery at all for the deep-etch device. In Fig. 9, the phase-shift change for a deep and shallow-etch device is shown again, but in this case, measurement procedure 3 was used and a forward current step during irradiation as well as during annealing was included in the measurement routine. During each measurement cycle, a 2-mA forward current was applied for 1 min before recording the optical spectra. First of all, a slight increase in the radiation tolerance can be seen when a forward current is applied during irradiation compared to both the procedure with (Fig. 5) and without (Fig. 8) I–V measurement. Furthermore, a full recovery of the phase shift can be seen for deep- and shallow-etch devices after 10 h of annealing time. The measurement of one arm of one MZM takes place every 31 min resulting in a total of 20 min at 42 mA necessary to reach full recovery. In addition to the recovery, the effect of reverse annealing also seems to be diminished as the phase shift returns to its preirradiation value which was not the case after annealing measurements with measurement procedure 1. In order to investigate the stability of the recovery and to prove that there is no reverse annealing effect with time, the phase shift was measured several times during the four months following irradiation using measurement procedure 2 and no degradation was observed. The first tests performed (mentioned in the beginning of this section) indicated that a current of 2 mA should be sufficient to completely recover the phase shift within 1 min. As shown in Fig. 9, this was not the case. For a complete recovery, several annealing steps were necessary. This leads to the hypothesis that the charge and trap density was higher in the measurement right after irradiation than that was in the case of the sample already stored for three months after irradiation, thus making longer annealing time or a higher forward current necessary. Further tests will show whether,

with a sufficiently high annealing current, the radiation damage can be compensated and if the phase-shift degradation during irradiation can be eliminated. A similar behavior has been described in MOSFETs by several groups [18]–[21]. While they all agree on the process of annealing being due to forward bias by electrons tunneling from the silicon to the interface and the oxide where they remove trapped holes, different explanations for the effect of reverse annealing due to application of reverse bias are given. Lelis *et al.* [18], [19] claim that in order to enable reversibility, there must be compensating electron traps produced along with the hole traps as part of the same complex. Electrons in that case solely compensate trapped holes rather than removing them permanently. Freitag *et al.* [21] instead support the theory of a two-defect model shown by Trombetta *et al.* [20] introducing the concept of reversible charge, which he calls "Anomalous Positive Charge" in addition to irreversible positive charge "trapped holes." Independent of the model explaining the reverse annealing effect, it might explain the slight degradation in phase shift after irradiation shown in Fig. 8. A summary of work done and more recent discussions to this topic can be found in [22], which emphasizes the importance of hydrogen in the oxide and its reaction with radiation-induced defects during and after irradiation.

IV. Conclusion

The influence of temperature on the radiation tolerance of custom-designed MZMs has been presented. It was shown that the radiation tolerance is significantly increased with decreasing temperature for deep- and shallow-etch devices. As the operating temperatures in the innermost regions of an HEP experiment where the radiation levels are highest are typically rather low, reaching -30 °C, these results are very promising in terms of increasing the survivability of SiPh MZMs in such environments. Furthermore, annealing results using different measurement procedures were shown and compared. Postirradiation measurements, including I–V curves at room temperature, showed a recovery of irradiated devices after they were stored unbiased for several months. In addition to an annealing effect at room temperature independent of biasing, it is most likely that the short forward bias applied during the I–V measurement included in the measurement procedure is responsible for the actual recovery. However, it appears that samples recovered with this method do not return to phase-shift values greater than 80% of their preirradiation values. Further annealing using longer period and/or higher magnitude forward current than while measuring I–V was shown to be a very effective annealing method. First of all, applying a forward current of 2 mA for 1 min every measurement cycle during irradiation led to an increase of radiation tolerance. Second, a full recovery of the phase shift could be achieved for all devices when measuring with the same procedure for only 10 h postirradiation. These results give hope for a significant increase of radiation tolerance of SiPh transmitters in the future HEP experiments if annealing steps are included in phases where operation is paused. Even though this would add some complexity to the driving circuit, it would have a negligible influence on the overall power efficiency of an optical link as the power needed is negligible in comparison with the power used by the driving electronics during normal operation. The observed irradiation and annealing effects could perhaps also be influenced by tuning the top oxide layer by, for example, using alternative materials or growth methods for the commonly used silicon dioxide insulation layer. However, the goal of this paper is to investigate the suitability of devices produced in standard foundry MPW processes. Thus, we are limited to the overlayer provided by the foundry. Further investigations are necessary to show whether the injection enhanced annealing behavior is generally applicable to other MZM structures. Should this be the case it opens up the possibility to use different MZMs optimized and offered by different foundries. In a next step, the effect of higher currents and longer annealing times during irradiation and annealing will be investigated for different MZM designs.

References

[1] G. Apollinari. (Jan. 2015). *High-Luminosity Large Hadron Collider (HL-LHC): Preliminary Design Report*. [Online]. Available: http://hilumilhc.web.cern.ch/about/hl-lhc-project

[2] J. Troska *et al.*, "Optical readout and control systems for the CMS tracker," *IEEE Trans. Nucl. Sci.*, vol. 50, no. 4, pp. 1067–1072, Aug. 2003.

[3] J. Troska, S. Detraz, S. S. El Nasr-storey, P. Stejskal, C. Sigaud, and C. Soos, "Radiation damage studies of lasers and photodiodes for use in multi-Gb/s optical data links," *IEEE Trans. Nucl. Sci.*, vol. 58, no. 6, pp. 3103–3110, Dec. 2011.

[4] S. S. El Nasr-Storey *et al.*, "Irradiation of new optoelectronic components for HL-LHC data transmission links," *J. Instrum.*, vol. 8, no. 12, p. C12040, Dec. 2013. [Online]. Available: http://stacks.iop.org/1748-0221/8/i=12/a=C12040?key=crossref.0b6f962f9e38047c3d88cae6bbe6cc77

[5] B. Milivojevic *et al.*, "112 Gb/s DP-QPSK transmission over 2427km SSMF using small-size silicon photonic IQ modulator and low-power CMOS driver," in *Proc. Opt. Fiber Commun. Conf./Nat. Fiber Opt. Engineers Conf.*, 2013, p. OTh1D.1. [Online]. Available: http://www.opticsinfobase.org/abstract.cfm?URI=OFC-2013-OTh1D.1

[6] M. Cignoli *et al.*, "A 1310 nm 3D-integrated silicon photonics Mach–Zehnder-based transmitter with 275 mW multistage CMOS driver achieving 6dB extinction ratio at 25Gb/s," *IEEE Int. Solid-State Circuits Conf. (ISSCC) Dig. Tech. Papers*, vol. 58. Feb. 2015, pp. 416–417.

[7] D. M. Gill *et al.*, "Monolithic travelling-wave Mach–Zehnder transmitter with high-swing stacked CMOS driver," in *Proc. CLEO*, Washington, DC, USA, 2014, p. SM2G.3. [Online]. Available: https://www.osapublishing.org/abstract.cfm?uri=CLEO_SI-2014-SM2G.3

[8] G. Casse *et al.*, "Thin silicon detectors for tracking in high radiation environments," in *Proc. IEEE Nucl. Sci. Symp. Conf. Rec.*, Oct. 2012, pp. 1661–1663.

[9] A. Candelori, "Radiation-hard detectors for very high luminosity colliders," *Nucl. Instrum. Methods Phys. Res. A, Accel. Spectrom. Detect. Assoc. Equip.*, vol. 560, no. 1, pp. 103–107, 2006.

[10] S. S. El Nasr-Storey *et al.*, "Silicon photonics for high energy physics data transmission applications," in *Proc. IEEE 11th Int. Conf. Group IV Photon. (GFP)*, Aug. 2014, pp. 1–2, doi: 10.1109/Group4.2014.6962056.

[11] S. S. El Nasr-Storey *et al.*, "Neutron and X-ray irradiation of silicon based Mach–Zehnder modulators," *J. Instrum.*, vol. 10, no. 3, p. C03040, Mar. 2015. [Online]. Available: http://stacks.iop.org/1748-0221/10/i=03/a=C03040?key=crossref.edfce1479893ba7a24d8e6dae43b6888

[12] S. S. El Nasr-Storey *et al.*, "Effect of radiation on a Mach–Zehnder interferometer silicon modulator for HL-LHC data transmission applications," *IEEE Trans. Nucl. Sci.*, vol. 62, no. 1, pp. 329–335, Feb. 2015.

[13] M. Zeiler *et al.*, "Design of Si-Photonic structures to evaluate their radiation hardness dependence on design parameters," *J. Instrum.*, vol. 11, no. 4, p. C01040, 2016.

[14] M. Zeiler *et al.*, "Radiation hardness evaluation and phase shift enhancement through ionizing radiation in silicon Mach–Zehnder modulators," in *Proc. Radiat. Effects Compon. Syst. (RADECS)*, Bremen, Germany, Sep. 2016, pp. 1–4, doi: 10.1109/RADECS.2016.8093130.

[15] P. Dumon, W. Bogaerts, R. Baets, J. M. Fedeli, and L. Fulbert, "Towards foundry approach for silicon photonics: Silicon photonics platform ePIXfab," *Electron. Lett.*, vol. 45, no. 12, pp. 581–582, Jun. 2009.

[16] M. Zeiler *et al.*, "A system-level model for high-speed, radiation-hard optical links in HEP experiments based on silicon Mach–Zehnder modulators," *J. Instrum.*, vol. 11, no. 12, p. C12059, 2016. [Online]. Available: http://stacks.iop.org/1748-0221/11/i=12/a=C12059?key=crossref.07dec4fa98cf77230fcea3b4d4d6ae97

[17] S. S. El Nasr-Storey *et al.*, "Modeling TID effects in Mach–Zehnder interferometer silicon modulator for HL-LHC data transmission applications," *IEEE Trans. Nucl. Sci.*, vol. 62, no. 6, pp. 2971–2978, Dec. 2015.

[18] A. J. Lelis, H. E. Boesch, T. R. Oldham, and F. B. McLean, "Reversibility of trapped hole annealing," *IEEE Trans. Nucl. Sci.*, vol. 35, no. 6, pp. 1186–1191, Dec. 1988. [Online]. Available: http://ieeexplore.ieee.org/document/25437/

[19] A. J. Lelis and T. R. Oldham, "Time dependence of switching oxide traps," *IEEE Trans. Nucl. Sci.*, vol. 41, no. 6, pp. 1835–1843, Dec. 1994. [Online]. Available: http://ieeexplore.ieee.org/document/340515/

[20] L. P. Trombetta, F. J. Feigl, and R. J. Zeto, "Positive charge generation in metal-oxide-semiconductor capacitors," *J. Appl. Phys.*, vol. 69, no. 4, pp. 2512–2521, Feb. 1991. [Online]. Available: http://aip.scitation.org/doi/10.1063/1.348689

[21] R. K. Freitag, D. B. Brown, and C. M. Dozier, "Experimental evidence of two species of radiation induced trapped positive charge," *IEEE Trans. Nucl. Sci.*, vol. 40, no. 6, pp. 1316–1322, Dec. 1993. [Online]. Available: http://ieeexplore.ieee.org/document/273536/

[22] D. M. Fleetwood, "Total ionizing dose effects in MOS and low-dose-rate-sensitive linear-bipolar devices," *IEEE Trans. Nucl. Sci.*, vol. 60, no. 3, pp. 1706–1730, Jun. 2013. [Online]. Available: http://ieeexplore.ieee.org/document/6522833/